

Anisotropy of Alfvénic Turbulence in the Solar Wind and Numerical Simulations

C. H. K. Chen,^{1*} A. Mallet,² T. A. Yousef,³ A. A. Schekochihin² and T. S. Horbury¹

¹*The Blackett Laboratory, Imperial College London, London SW7 2AZ, United Kingdom*

²*Rudolf Peierls Centre for Theoretical Physics, University of Oxford, Oxford OX1 3NP, United Kingdom*

³*Bjørn Stallars gt 1, 7042 Trondheim, Norway*

2010 September 3

ABSTRACT

We investigate the anisotropy of Alfvénic turbulence in the inertial range of the solar wind and in both driven and decaying reduced magnetohydrodynamic simulations. A direct comparison is made by measuring the anisotropic second order structure functions in both data sets. In the solar wind, the perpendicular spectral index of the magnetic field is close to $-5/3$. In the forced simulation, it is close to $-5/3$ for the velocity and $-3/2$ for the magnetic field. In the decaying simulation, it is $-5/3$ for both fields. The spectral index becomes steeper at small angles to the local magnetic field direction in all cases. We also show that when using the global rather than local mean field, the anisotropic scaling cannot be measured.

Key words: magnetic fields – (magnetohydrodynamics) MHD – plasmas – solar wind – turbulence

1 INTRODUCTION

The solar wind is a turbulent plasma with a power spectrum extending over many orders of magnitude (e.g., Coleman 1968). Scales larger than the ion gyroradius are considered to be the inertial range, and the spectral indices are observed to be close to $-5/3$ for the magnetic and electric fields and $-3/2$ for velocity (e.g., Matthaeus & Goldstein 1982; Bale et al. 2005; Podesta et al. 2007; Tessein et al. 2009). There is also evidence that the fluctuations are predominantly Alfvénic (e.g., Belcher & Davis 1971; Horbury et al. 1995; Bale et al. 2005).

Solar wind turbulence is anisotropic with respect to the direction of the magnetic field. For example, the magnetic field correlation length has been shown to vary depending on the angle of observation with respect to the field direction (Crooker et al. 1982; Matthaeus et al. 1990; Dasso et al. 2005; Osman & Horbury 2007; Weygand et al. 2009). The magnetic field power and spectral indices are also observed to be anisotropic: power at a fixed scale increases with angle to the magnetic field (Bieber et al. 1996; Osman & Horbury 2009) and the spectral index varies from -2 at small angles to between $-3/2$ and $-5/3$ in the field perpendicular direction (Horbury et al. 2008; Podesta 2009; Wicks et al. 2010; Luo & Wu 2010). These observations are consistent with theories of critically balanced MHD turbulence, for example, that of Goldreich & Sridhar (1995), which predicts anisotropic fluctuations ($k_{\perp} > k_{\parallel}$) and the -2 and $-5/3$ spectral indices.

Simulations of plasma turbulence have also been performed, most of which have used the equations of incompressible magne-

tohydrodynamics (MHD). When a strong mean field is present, the spectral index is closer to $-3/2$ than $-5/3$ (Maron & Goldreich 2001; Müller et al. 2003; Müller & Grappin 2005; Mason et al. 2008; Perez & Boldyrev 2008), although a limited inertial range and the bottleneck effect (Falkovich 1994) make this number hard to determine precisely (Beresnyak & Lazarian 2009).

Anisotropy has also been measured in MHD simulations. Early 2D simulations showed that the turbulence developed wavevector anisotropy so that the fluctuations had $k_{\perp} > k_{\parallel}$ (Shebalin et al. 1983), and this was later confirmed in 3D simulations (Oughton et al. 1994; Matthaeus et al. 1996; Milano et al. 2001). The anisotropy was also measured to be scale dependent, such that $k_{\parallel} \sim k_{\perp}^{2/3}$ (Cho & Vishniac 2000; Maron & Goldreich 2001), in agreement with the critical balance predictions (Goldreich & Sridhar 1995). An important point noted in these studies, and also in solar wind measurements (Horbury et al. 2008), was that the anisotropic scaling is with respect to the scale dependent local field and not the global mean field.

The theory of Goldreich & Sridhar (1995) was extended by Boldyrev (2006) to account for a phenomenon called dynamic alignment. In this theory, the velocity and magnetic field fluctuations align to within a scale dependent angle and the perpendicular spectral index becomes $-3/2$. There is evidence for this scale dependent alignment in the solar wind (Podesta et al. 2009) and driven MHD simulations (Mason et al. 2006, 2008).

To date, there has not been a measurement of the spectral index parallel to the local magnetic field in simulations. Measurements of the perpendicular spectral index in the solar wind and simulations are also not always in agreement. It is important to be sure

* E-mail: christopher.chen03@imperial.ac.uk

Table 1. Mean parameter values for the 65 solar wind intervals

SW Speed (v_{sw})	$360 \pm 10 \text{ km s}^{-1}$
Ion number density (n_i)	$8.6 \pm 0.4 \text{ cm}^{-3}$
Alfvén Speed (v_A)	$40 \pm 2 \text{ km s}^{-1}$
Perpendicular Ion Temperature ($T_{i\perp}$)	$7.5 \pm 0.4 \text{ eV}$
Ion Beta (β_i)	1.1 ± 0.1
Ion Temperature Anisotropy ($T_{i\perp}/T_{i\parallel}$)	0.5 ± 0.2
Ion Gyroradius (ρ_i)	$74 \pm 3 \text{ km}$
Alfvén ratio (r_A)	0.72 ± 0.04

that the same quantities are being measured in both the solar wind and simulations and the subject of this paper is such a comparative study. We apply a similar analysis technique to both solar wind data and reduced MHD (RMHD) simulations, to make a direct comparison of the anisotropic scaling. In Section 2 we present the solar wind analysis, in Section 3 we present the simulation analysis, and Section 4 we discuss our conclusions.

2 INERTIAL RANGE SOLAR WIND MEASUREMENTS

2.1 Data Intervals

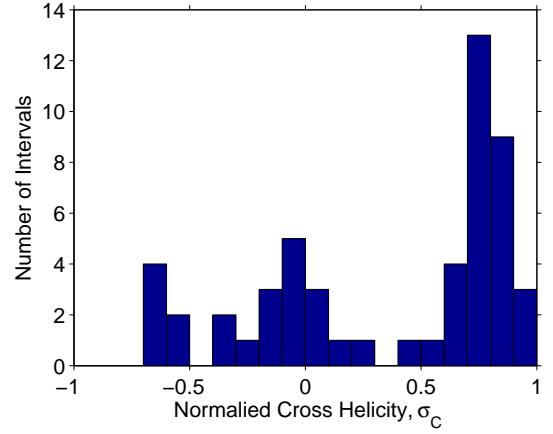
In this section, we apply the multi-spacecraft method of Chen et al. (2010a) to obtain the power and spectral index anisotropy of inertial range turbulence in the slow solar wind. The technique is applied to 65 1-hour intervals of data from the Cluster spacecraft (Escoubet et al. 2001) from 2006, when the separation between the four spacecraft was $\sim 10,000 \text{ km}$. In all of the intervals, the solar wind speed was $< 550 \text{ km s}^{-1}$. We use 4 s measurements of the magnetic field from the fluxgate magnetometer (FGM) (Balogh et al. 2001) and velocity and density moments from the Cluster ion spectrometer (CIS) (Rème et al. 2001). The Cluster spacecraft are 1 AU from the Sun and the selected intervals are in pure solar wind with no evidence of ion foreshock activity.

The mean values of various parameters for the chosen intervals are given in Table 1. The geometric mean is used for the ion beta, temperature anisotropy, gyroradius and Alfvén ratio. The Alfvén ratio is the ratio of energy in the velocity fluctuations to the magnetic fluctuations, $r_A = E^v/E^b$, where the magnetic fluctuations are in Alfvén units. We have calculated this in the spacecraft frequency range $2 \times 10^{-3} \text{ Hz}$ to $1 \times 10^{-2} \text{ Hz}$, which roughly corresponds to scales 36,000 km to 180,000 km. While this is at larger scales than our anisotropy measurements, it is in the range where noise does not appear to dominate the velocity spectra. The value slightly less than unity that we obtain (≈ 0.7) is consistent with previous measurements (e.g., Matthaeus & Goldstein 1982; Bavassano et al. 1998; Podesta et al. 2007; Salem et al. 2009).

We also calculate the normalised cross helicity, σ_C , in each interval over the same range using the usual convention that positive values correspond to Alfvénic propagation away from the Sun. A histogram of σ_C (Fig. 1) shows a range of values with a non-Gaussian distribution: there is a large outward population ($\sigma_C > 0.5$), a balanced population ($\sigma_C \approx 0$), and a few inward intervals ($\sigma_C < -0.5$).

2.2 Analysis Technique

For each interval, pairs of points from the time series of the four spacecraft are used to calculate second order structure functions at

**Figure 1.** Histogram of normalised cross helicity, σ_C , for the slow solar wind intervals, in the spacecraft frequency range $2 \times 10^{-3} \text{ Hz}$ to $1 \times 10^{-2} \text{ Hz}$.

different angles to the local magnetic field (Chen et al. 2010a). The structure function is defined as

$$\delta B_i^2(\mathbf{l}) = \langle |B_i(\mathbf{r} + \mathbf{l}) - B_i(\mathbf{r})|^2 \rangle, \quad (1)$$

where B_i is the i th component of the magnetic field, \mathbf{l} is the separation vector, and the angular brackets denote an ensemble average over positions \mathbf{r} . The local mean magnetic field is defined as

$$\mathbf{B}_{\text{local}} = \frac{\mathbf{B}(\mathbf{r} + \mathbf{l}) + \mathbf{B}(\mathbf{r})}{2}. \quad (2)$$

We calculate the structure functions of the local perpendicular magnetic field component, \mathbf{B}_{\perp} , which corresponds to the Alfvénic fluctuations.

The structure function values are binned according to scale parallel, l_{\parallel} , and perpendicular, l_{\perp} , to $\mathbf{B}_{\text{local}}$. The bins cover the range 2,000 km to 20,000 km, which is within, although towards the small scale end, of the inertial range. The result of this binning for one of the 65 intervals is shown in Fig. 2. Although single intervals are noisy, it can be seen that the contours are elongated in the field parallel direction. This indicates that the eddies are anisotropic with $k_{\perp} > k_{\parallel}$.

The data is also binned according to scale l and the angle θ_B between \mathbf{l} and $\mathbf{B}_{\text{local}}$. Straight lines, in log-log space, are then fitted to the structure functions for each θ_B bin and the power anisotropy is obtained by evaluating these fits at a scale of 10,000 km. The spectral index at each θ_B is found using the relation $\alpha = g + 1$, where $-\alpha$ is the spectral index and g is the structure function scaling exponent (Monin & Yaglom 1975). This is similar to the work of Osman & Horbury (2009), except we bin the data with respect to the *local* field direction, since this appears to be the relevant mean field for the fluctuations, and we use many more intervals.

2.3 Magnetic Field Anisotropy

The results, averaged over all 65 slow wind intervals, are shown in Fig. 3. The error bars are the standard error on the mean from averaging the intervals. They confirm previous observations in the fast wind that show power increasing with θ_B and a variation in spectral index from -2 at small angles to between $-5/3$ and $-3/2$ at large angles (Horbury et al. 2008; Podesta 2009; Wicks et al. 2010; Luo & Wu 2010). Our multi-spacecraft technique, therefore, produces results that agree with these single spacecraft measurements.

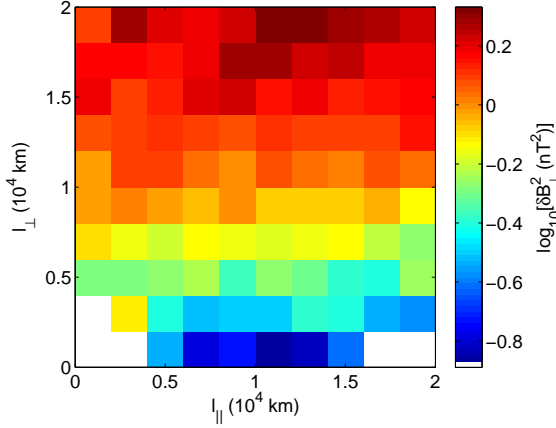


Figure 2. Second order structure function of the perpendicular magnetic field component for one of the 65 solar wind intervals as a function of parallel (l_{\parallel}) and perpendicular (l_{\perp}) separation.

The power anisotropy is consistent with eddies elongated along the local magnetic field direction and wavevector anisotropy of the form $k_{\perp} > k_{\parallel}$ (Chen et al. 2010b). The perpendicular spectral index that we obtain here (for $20^\circ < \theta_B < 90^\circ$) is closer to $-5/3$ than $-3/2$. This fits the prediction of Goldreich & Sridhar (1995), rather than Boldyrev (2006). Both of these theories, however, apply to balanced turbulence, i.e., $\sigma_C = 0$. As can be seen from Fig. 1, many of the intervals have large σ_C . This is common in the solar wind and different theories of imbalanced MHD turbulence have been proposed (e.g., Lithwick et al. 2007; Chandran 2008; Beresnyak & Lazarian 2008; Perez & Boldyrev 2009; Podesta & Bhattacharjee 2010). Differentiating between these, however, is beyond the scope of this paper.

In the next section, we apply a similar analysis to RMHD simulations. This enables a direct comparison to be made between turbulence in the solar wind and numerical simulations.

3 REDUCED MHD SIMULATIONS

3.1 Simulation Description

The RMHD equations, originally derived by Strauss (1976), can be written in Elsasser potentials (Schekochihin et al. 2009),

$$\begin{aligned} \frac{\partial}{\partial t} \nabla_{\perp}^2 \zeta^{\pm} \mp v_A \nabla_{\parallel} \nabla_{\perp}^2 \zeta^{\pm} \\ = -\frac{1}{2} [\{\zeta^+, \nabla_{\perp}^2 \zeta^-\} + \{\zeta^-, \nabla_{\perp}^2 \zeta^+\} \mp \nabla_{\perp}^2 \{\zeta^+, \zeta^-\}], \end{aligned} \quad (3)$$

where $\{A, B\} = \hat{\mathbf{b}}_0 \cdot (\nabla_{\perp} A \times \nabla_{\perp} B)$, $\hat{\mathbf{b}}_0$ is the mean field unit vector and v_A is the Alfvén speed. The Elsasser potentials are defined as $\mathbf{z}^{\pm} = \hat{\mathbf{b}}_0 \times \nabla_{\perp} \zeta^{\pm}$ and the Elsasser variables are $\mathbf{z}^{\pm} = \mathbf{v} \pm \mathbf{b}$, where \mathbf{v} is the velocity and \mathbf{b} is the magnetic field in Alfvén units.

The equations contain only the perpendicular fluctuations and are, therefore, suitable for simulating Alfvénic turbulence. They are also more efficient to simulate than full MHD, since they involve only two scalar fields. Although originally derived from MHD, it has been shown that RMHD can be derived for a collisionless plasma such as the solar wind (Schekochihin et al. 2009). The derivation assumes anisotropy ($k_{\perp} \gg k_{\parallel}$) and a strong mean field ($B_0 \gg \delta B_{\perp}$), both of which are observed at the smaller scale end of the solar wind inertial range.

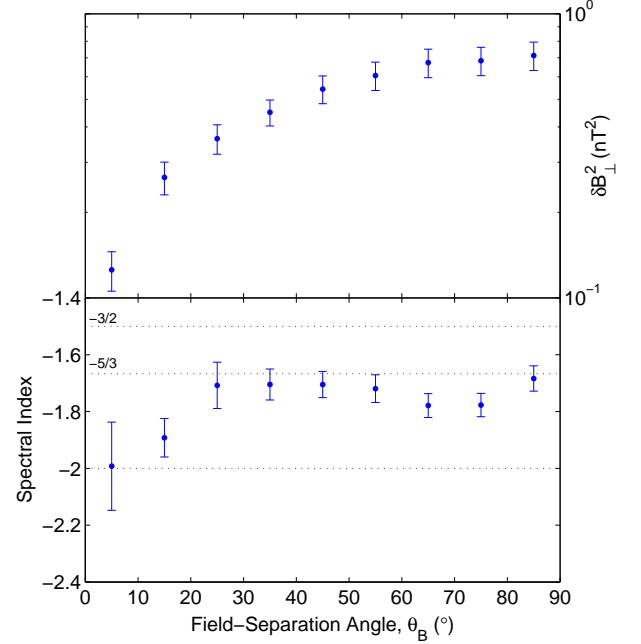


Figure 3. Power and spectral index anisotropy of the magnetic field in inertial range turbulence in the slow solar wind. The power anisotropy is calculated at $l = 10,000$ km. Spectral index values of $-3/2$, $-5/3$ and -2 are given as dotted lines for reference.

The simulation reported here solves the RMHD equations in a triply periodic cube of size $(2\pi)^3$ with a resolution of 512^3 . The Alfvén speed is set to $v_A = 1$ (making the Alfvén crossing time 2π). It can be seen from Eq. 3 that if the Alfvén speed is scaled by a factor R and the z coordinate, which is the mean field direction, is also scaled by R then the equations remain identical. This means that our simulations correspond to all values of R , and therefore all values of $\delta B_{\perp}/B_0$ if the box is also stretched in the parallel direction by R . The units of length in the perpendicular and parallel directions, therefore, are independent of each other in RMHD. This is because the anisotropy is formally infinite and the fluctuation level is infinitely small under the RMHD asymptotic expansion. Choosing a value of R sets the anisotropy and mean field strength so that the simulations can be compared to a real world situation.

The equations are solved pseudospectrally in x and y , and using a centred finite difference scheme in z . In the x and y directions, a 4th order hyperviscosity (∇_{\perp}^8) dissipation term is used, while in the z direction a very small Laplacian viscosity (∇_{\parallel}^2) is added to keep the high k_z modes from becoming unstable. The simulation is initially forced in velocity on large scales ($k_{\perp} = 1, 2$ and $k_z = 1$) with a Gaussian white noise forcing. We choose to force only the velocity field to match possible sources of solar wind forcing, such as velocity shears or large scale Alfvén waves. There is no known mechanism of breaking magnetic flux conservation at large scales, so we do not force the magnetic field. After a while, the forcing is turned off and the simulation is left to freely decay.

A time series of various parameters is shown in Fig. 4. The turnover time of the largest eddies is ~ 5 . The transition between the forced and decaying parts of the simulation can clearly be seen in the Elsasser variable RMS values (upper panel) at $t = 28$. The normalised cross helicity σ_C , the Alfvén ratio r_A , and the spectral

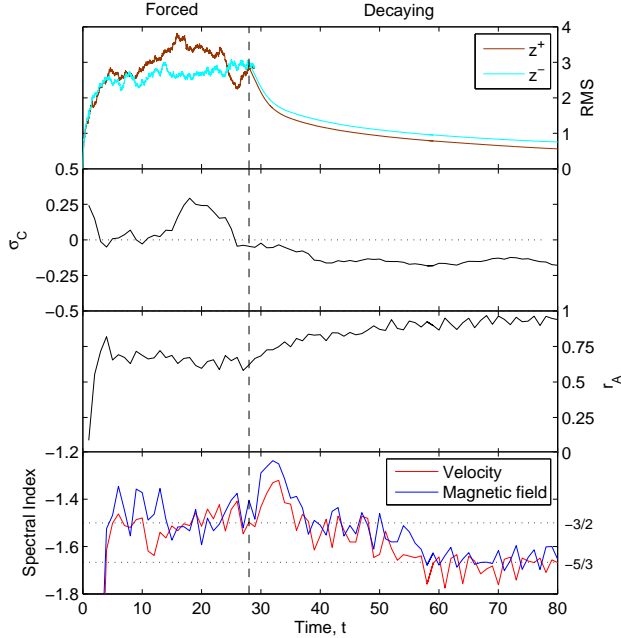


Figure 4. Time series of various parameters in the simulation: RMS Elsasser variables, normalised cross helicity σ_C , Alfvén ratio r_A and Fourier spectral indices. For $t \leq 28$ the simulation is forced and for $t > 28$ it is decaying. Spectral index values of $-3/2$ and $-5/3$ are given as dotted lines for reference in the lower panel.

indices in Fig. 4 are calculated over the range $k = 7$ to $k = 33$. During the forced period, σ_C fluctuates around 0. When the forcing is removed, it then decreases towards -1 , as expected from dynamic alignment theory (Dobrowolny et al. 1980). The decrease is fairly slow: σ_C changes from -0.045 at $t = 28$ to -0.13 at $t = 78$.

During the forced period $r_A \approx 0.66$, which is similar to solar wind observations (Table 1). As the simulation decays, r_A grows and approaches unity. This equipartition of energy is expected for MHD turbulence (Kraichnan 1965). The fact that the equipartition occurs only in the decaying period suggests that observations of $r_A < 1$ in simulations (e.g., Beresnyak & Lazarian 2006) and the solar wind (e.g., Matthaeus & Goldstein 1982; Bavassano et al. 1998; Podesta et al. 2007; Salem et al. 2009) may be due to effects of large scale forcing.

The spectral indices for the velocity and magnetic field are shown in the lower panel of Fig. 4. These are calculated from the gradients of the best fit lines to the perpendicular energy spectrum in log-log space. During the forced period, they are closer to $-3/2$ than $-5/3$, in agreement with previous results (Maron & Goldreich 2001; Müller et al. 2003; Müller & Grappin 2005; Mason et al. 2008; Perez & Boldyrev 2008). When the forcing is removed, however, they gradually steepen and appear to reach a steady value of $-5/3$ from $t = 58$ onwards.

In the following analysis we investigate the anisotropic scaling in the forced period $4 \leq t \leq 28$, and the decaying period $58 \leq t \leq 78$. We assume that in each of these periods the turbulence is stationary and we can perform averages over them. The averaged power spectra are shown in Fig. 5. The decaying spectra are normalised to their values at $t = 58$ before averaging. Gradients of $-5/3$ and $-3/2$ are given for reference, although it is hard to

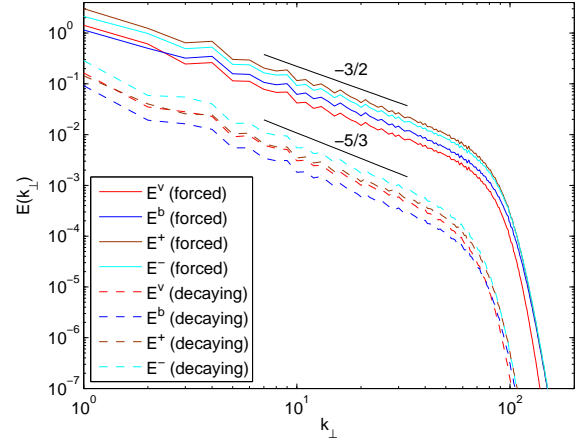


Figure 5. Perpendicular power spectra of velocity (E^v), magnetic field (E^b), and Elsasser variables (E^+ and E^-) in the forced and decaying periods of the simulation. $-5/3$ and $-3/2$ slopes are given for reference.

tell the the difference between these visually. It can be seen that between $k_\perp = 7$ and $k_\perp = 33$ there are well defined power laws in all the spectra.

3.2 Analysis Technique

The technique we use to analyse the simulation data is similar to that used in Section 2.2, with modifications to account for the simulation geometry. Firstly, the scaling factor R , which should be bigger than 1 for the RMHD equations to be valid, is chosen. Here, we set $R = 4$, which is a compromise between typical solar wind wavevector anisotropies of between 2 and 3 (Wicks et al. 2010; Chen et al. 2010b) and $\delta \mathbf{B}/B_0$ values, which are on average around 0.1 (Smith et al. 2006). This means that our box is stretched by a factor of 4 in the parallel direction and the Alfvén speed is set to 4.

For a particular snapshot in time, many pairs of points in the simulation box are picked at random. The second order structure function values of the local perpendicular velocity and magnetic field components are calculated and binned, as in Section 2.2. The structure function of the magnetic field binned with respect to l_\parallel and l_\perp at $t = 28$ is shown in Fig. 6. It is representative of the velocity and magnetic field structure functions in both the forced and decaying periods of the simulation. Similarly to the solar wind (Fig. 2) and previous simulations (Cho & Vishniac 2000), the contours are elongated in the parallel direction.

In the range $0.35 \leq l \leq 1.3$, which corresponds approximately to $5 \leq k \leq 18$, the structure functions are approximately power laws and we assume this to be the inertial range of the simulation. The spectral indices and the power anisotropy (calculated at $l = 0.8$) are found from the best fit lines to the data binned with respect to l and θ_B in this range. This is done for snapshots separated by 2 time units, giving 13 snapshots for the forced period and 11 for the decaying period.

3.3 Power and Spectral Index Anisotropy

The power and spectral index anisotropy for the velocity and magnetic field are shown in Fig. 7. The error bars are the standard error on the mean from averaging the results of the snapshots in each period. In both cases, the power increases with angle to the local mag-

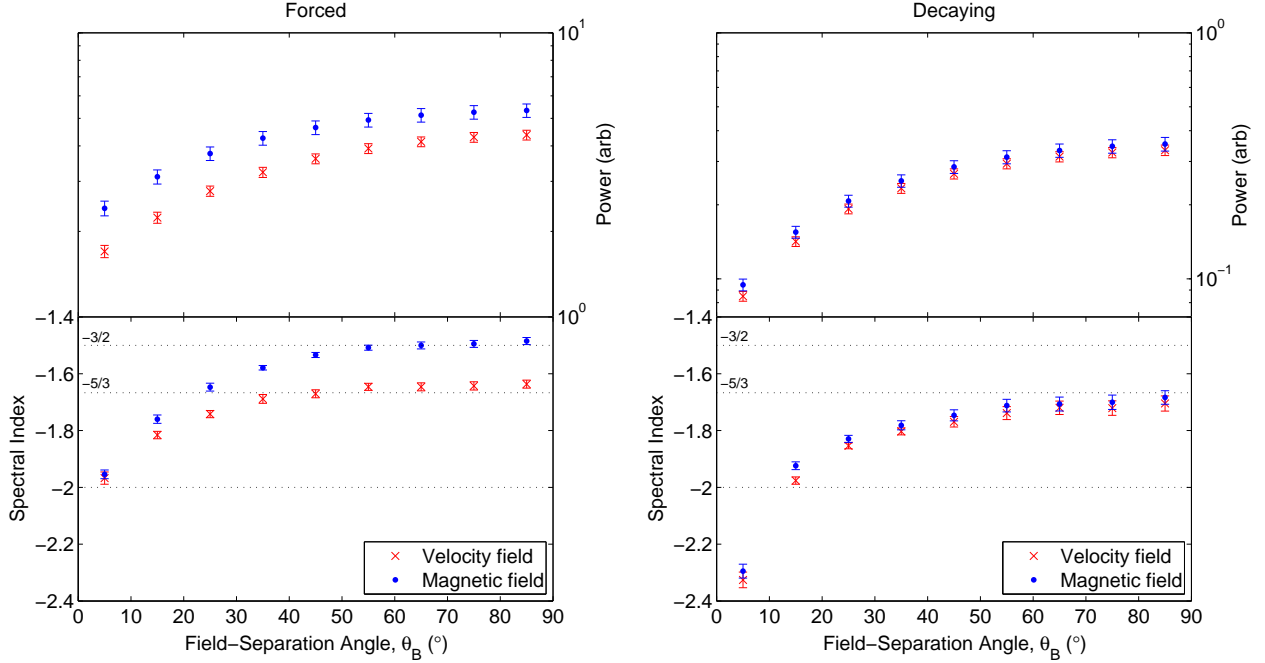


Figure 7. Anisotropy of forced (left) and decaying (right) simulations. Power (top panels) and spectral index (bottom panels) with respect to the local magnetic field direction for the velocity and magnetic field are shown. The power anisotropy is calculated at $l = 0.8$.

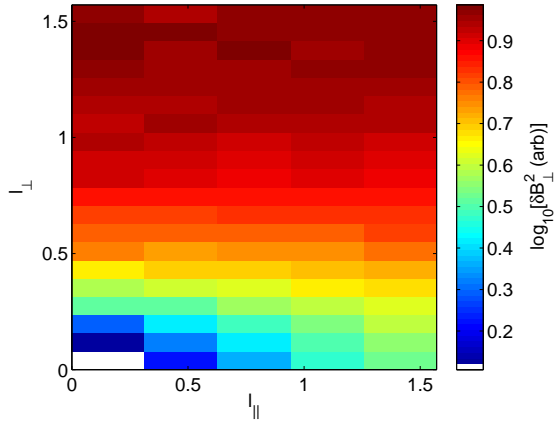


Figure 6. Second order structure function of the perpendicular magnetic field component for one of the snapshots ($t = 28$) in the forced simulation as a function of parallel (l_\parallel) and perpendicular (l_\perp) separation.

netic field θ_B , as it does in the solar wind. For the forced case, the overall power in the magnetic field is larger than that in the velocity, whereas in the decaying case they are similar. This is consistent with our previous discussion of the Alfvén ratio being $r_A < 1$ in the forced case and $r_A \approx 1$ in the decaying case. It is also interesting to note that these curves are qualitatively similar in shape. No prediction for this shape has yet been made based on critical balance theory.

In the forced case, there is a difference between the spectral index anisotropy of the velocity and magnetic field. The velocity spectral index varies from -2 at small θ_B to $-5/3$ at large θ_B . The magnetic field spectral index is also -2 at small θ_B but is less

steep at larger θ_B , having a value close to $-3/2$. The fact that both are steep at small angles shows that the turbulence is anisotropic and the -2 scaling is consistent with the critical balance theories of both Goldreich & Sridhar (1995) and Boldyrev (2006). The difference at large angles, however, is unexpected, since theories of Alfvénic turbulence predict that they scale in the same way. The velocity scaling matches the predictions of Goldreich & Sridhar (1995) and the magnetic field scaling matches the predictions of Boldyrev (2006).

For the decaying case, both fields show similar scaling. The spectral index is close to $-5/3$ for large θ_B and much steeper at small θ_B : -2.33 ± 0.03 for velocity and -2.30 ± 0.03 for the magnetic field. Again, the steepening at low θ_B shows the turbulence is anisotropic, although the spectra are steeper than the critical balance prediction of -2 . One possible explanation for this is that the turbulence may be transitioning to the weak regime, in which there is not thought to be a parallel cascade (Goldreich & Sridhar 1997; Galtier et al. 2000). Perez & Boldyrev (2008) observed the perpendicular spectral index steepening as the turbulence became weaker, and we may be observing a similar effect for the parallel index. In a different run (not shown here) that was forced less strongly, we observed overall steeper spectral indices at all angles. The perpendicular spectral index, however, seems to remain at $-5/3$ for many turnover times in the run here (Fig. 4), rather than dropping to -2 as expected for weak turbulence.

We now compare the spectral indices obtained through the structure function technique to the Fourier indices. The time series of the global perpendicular Fourier indices are shown in the lower panel of Fig. 4. It can be seen that both fields have spectral indices close to $-3/2$ during the forced period and then after a transition, reach a value of $-5/3$ in the decaying period. The mean values are -1.51 ± 0.01 for the velocity and -1.47 ± 0.01 for the magnetic field in the forced case and -1.69 ± 0.01 for the velocity and

-1.653 ± 0.007 for the magnetic field in the decaying case. These are consistent with the perpendicular spectral indices measured using structure functions, except for velocity in the forced case, which is close to $-5/3$. It is possible that this difference is caused by the velocity forcing, which is localised in Fourier space, but may affect the structure function, which mixes small and large scale information (Davidson & Pearson 2005).

The results we obtain here are broadly consistent with previous simulations. Wavevector anisotropy of the form $k_{\perp} > k_{\parallel}$ has been observed previously (Shebalin et al. 1983; Oughton et al. 1994; Matthaeus et al. 1996; Milano et al. 2001). In particular, Cho & Vishniac (2000) observed a difference in anisotropic scaling between the velocity and magnetic field in their forced simulations. When the mean field was of a similar strength to the RMS fluctuations they obtained $k_{\parallel} \sim k_{\perp}^{0.7}$ for velocity but $k_{\parallel} \sim k_{\perp}^{0.5}$ for the magnetic field.

We now compare the simulation and solar wind results. Firstly we note that both sets of results are qualitatively similar. Power at a fixed scale is anisotropic and increases as θ_B increases. All spectral index curves are anisotropic and steepen at small θ_B as predicted by critical balance theories. The main difference between the solar wind and simulations is the value of the perpendicular spectral index. For the magnetic field, we observe $-5/3$ in the solar wind and the decaying simulation but $-3/2$ in the forced simulation. Both $-5/3$ and $-3/2$ have been observed previously in the solar wind (Horbury et al. 2008; Podesta 2009; Wicks et al. 2010; Luo & Wu 2010). In both our forced and decaying simulations the velocity has a perpendicular index of $-5/3$. Solar wind measurements, however, suggest that it is closer to $-3/2$ (Podesta et al. 2007; Tessein et al. 2009). These differences in perpendicular spectral index are a currently unresolved issue in solar wind turbulence.

3.4 Local vs Global Mean Field

Finally, we investigate the difference between using the local and global magnetic field for defining the mean field for the fluctuations. Fig. 8 shows the anisotropy of power and scaling in velocity from the forced period of the simulation using the local mean field method described previously. Also plotted is the anisotropy of power and scaling using, instead, the global mean field. In other words, the structure functions are binned according to the separation direction with respect to the average field direction over the whole simulation box (the z direction).

It can be seen that when using the global mean field method, the spectral index is much less anisotropic, i.e., at small θ_B it only reaches a value of -1.76 ± 0.02 rather than -1.97 ± 0.02 with the local field method. This is because the magnetic field fluctuations are large enough that the local field direction seen by an eddy is not the same as the large scale global field direction. If the fluctuations are in critical balance, the angle between the local and global mean fields is $\delta \mathbf{B}_{\perp}/B_0 \approx k_{\parallel}/k_{\perp}$. This suggests that when using the global mean field, the parallel scaling can not be measured, even for small $\delta \mathbf{B}_{\perp}/B_0$, because the angle of measurement to the local field needs to be much less than k_{\parallel}/k_{\perp} .

This interpretation is in agreement with previous solar wind studies that have used local and global mean field methods. Those that use the global field method do not detect spectral index anisotropy (Sari & Valley 1976; Tessein et al. 2009) and those that use a local mean field method do detect it (Horbury et al. 2008; Podesta 2009; Wicks et al. 2010; Luo & Wu 2010). A similar situation is also seen in other simulations, where scaling anisotropy

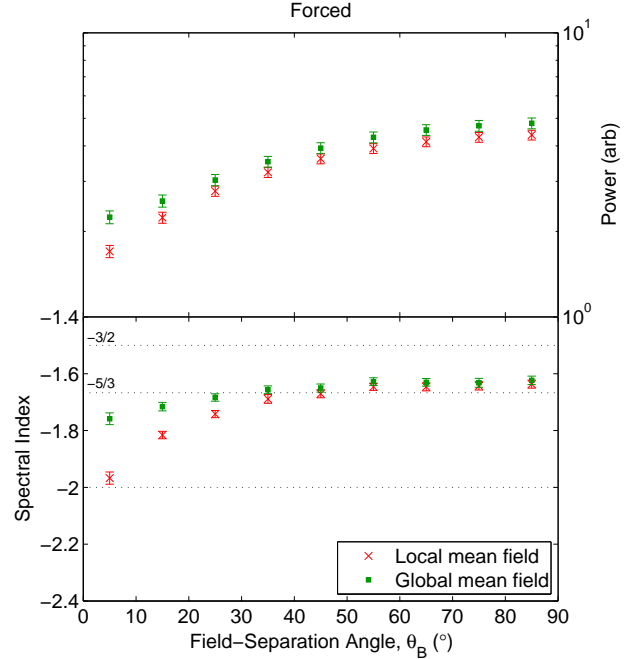


Figure 8. Power and spectral index anisotropy of velocity in the forced simulation using local and global mean field methods. The power anisotropy is calculated at $l = 0.8$.

is detected when a local mean field is used (Cho & Vishniac 2000; Maron & Goldreich 2001) but not when a global mean field is used (Grappin & Müller 2010). It seems, therefore, that the Alfvénic fluctuations, both in solar wind turbulence and MHD simulations, are not sensitive to the global large scale field, but to the local field at the scale of the fluctuations.

4 SUMMARY AND CONCLUSIONS

In this paper, we measure the power and spectral index anisotropy of Alfvénic turbulence in the solar wind and RMHD simulations using second order structure functions. The technique is essentially the same for both, allowing us to make a direct comparison. In the solar wind, we find that the magnetic field power and spectral index are anisotropic with respect to the local magnetic field direction. This anisotropy has now been seen by several different methods. In both forced and decaying simulations we also find that the power and spectral index are anisotropic in both the velocity and magnetic field.

In the solar wind, the perpendicular spectral index of the magnetic field is close to $-5/3$, in agreement with the predictions of Goldreich & Sridhar (1995). In the forced simulation, the perpendicular spectral indices are close to $-5/3$ for velocity and $-3/2$ for the magnetic field. We are not aware of any theory that can account for this difference. In the decaying simulation, the perpendicular spectral index is close to $-5/3$ for both the velocity and magnetic field. In all cases, the spectral index steepens at small angles to the magnetic field. The parallel scaling obtained in the solar wind and forced simulations is close to -2 , which agrees with the theories based on critical balance of both Goldreich & Sridhar (1995) and Boldyrev (2006). The parallel spectral indices in the decaying simulation are -2.33 ± 0.03 for the velocity and -2.30 ± 0.03 for the

magnetic field, which are steeper than the critical balance predictions.

We also find that when measuring the anisotropy of the fluctuations in the forced simulation with respect to the global magnetic field, rather than the local mean field, the spectral index is much less anisotropic, with a value of -1.76 ± 0.02 in the parallel direction. This suggests that the turbulence is only anisotropic with respect to the local magnetic field. This is consistent with previous solar wind and simulation results; those that use the local mean field see anisotropic scaling and those that use the global field do not.

ACKNOWLEDGMENTS

This work was supported by STFC and the Leverhulme Trust Network for Magnetized Plasma Turbulence. FGM and CIS data was obtained from the Cluster Active Archive. The simulations were carried out using resources at the Texas Advanced Computing Center. C. Chen acknowledges useful conversations with R. Wicks.

REFERENCES

- Bale S. D., Kellogg P. J., Mozer F. S., Horbury T. S., Reme H., 2005, *Phys. Rev. Lett.*, 94, 215002
- Balogh A., Carr C. M., Acuña M. H., Dunlop M. W., Beek T. J., Brown P., Fornaçon K.-H., Georgescu E., Glassmeier K.-H., Harris J., Musmann G., Oddy T., Schwingenschuh K., 2001, *Ann. Geophys.*, 19, 1207
- Bavassano B., Pietropaolo E., Bruno R., 1998, *J. Geophys. Res.*, 103, 6521
- Belcher J. W., Davis L., 1971, *J. Geophys. Res.*, 76, 3534
- Beresnyak A., Lazarian A., 2006, *ApJ*, 640, L175
- Beresnyak A., Lazarian A., 2008, *ApJ*, 682, 1070
- Beresnyak A., Lazarian A., 2009, *ApJ*, 702, 1190
- Bieber J. W., Wanner W., Matthaeus W. H., 1996, *J. Geophys. Res.*, 101, 2511
- Boldyrev S., 2006, *Phys. Rev. Lett.*, 96, 115002
- Chandran B. D. G., 2008, *ApJ*, 685, 646
- Chen C. H. K., Horbury T. S., Schekochihin A. A., Wicks R. T., Alexndrova O., Mitchell J., 2010a, *Phys. Rev. Lett.*, 104, 255002
- Chen C. H. K., Wicks R. T., Horbury T. S., Schekochihin A. A., 2010b, *ApJ*, 711, L79
- Cho J., Vishniac E. T., 2000, *ApJ*, 539, 273
- Coleman P. J., 1968, *ApJ*, 153, 371
- Crooker N. U., Siscoe G. L., Russell C. T., Smith E. J., 1982, *J. Geophys. Res.*, 87, 2224
- Dasso S., Milano L. J., Matthaeus W. H., Smith C. W., 2005, *ApJ*, 635, L181
- Davidson P. A., Pearson B. R., 2005, *Phys. Rev. Lett.*, 95, 214501
- Dobrowolny M., Mangeney A., Veltri P., 1980, *Phys. Rev. Lett.*, 45, 144
- Escoubet C. P., Fehringer M., Goldstein M., 2001, *Ann. Geophys.*, 19, 1197
- Falkovich G., 1994, *Phys. Fluids*, 6, 1411
- Galtier S., Nazarenko S. V., Newell A. C., Pouquet A., 2000, *J. Plasma Phys.*, 63, 447
- Goldreich P., Sridhar S., 1995, *ApJ*, 438, 763
- Goldreich P., Sridhar S., 1997, *ApJ*, 485, 680
- Grappin R., Müller W., 2010, arXiv:1008.0727v1
- Horbury T. S., Balogh A., Forsyth R. J., Smith E. J., 1995, *Geophys. Res. Lett.*, 22, 3405
- Horbury T. S., Forman M., Oughton S., 2008, *Phys. Rev. Lett.*, 101, 175005
- Kraichnan R. H., 1965, *Phys. Fluids*, 8, 1385
- Lithwick Y., Goldreich P., Sridhar S., 2007, *ApJ*, 655, 269
- Luo Q. Y., Wu D. J., 2010, *ApJ*, 714, L138
- Maron J., Goldreich P., 2001, *ApJ*, 554, 1175
- Mason J., Cattaneo F., Boldyrev S., 2006, *Phys. Rev. Lett.*, 97, 255002
- Mason J., Cattaneo F., Boldyrev S., 2008, *Phys. Rev. E*, 77, 036403
- Matthaeus W. H., Ghosh S., Oughton S., Roberts D. A., 1996, *J. Geophys. Res.*, 101, 7619
- Matthaeus W. H., Goldstein M. L., 1982, *J. Geophys. Res.*, 87, 6011
- Matthaeus W. H., Goldstein M. L., Roberts D. A., 1990, *J. Geophys. Res.*, 95, 20673
- Milano L. J., Matthaeus W. H., Dmitruk P., Montgomery D. C., 2001, *Phys. Plasmas*, 8, 2673
- Monin A. S., Yaglom A. M., 1975, *Statistical Fluid Mechanics*, Vol 2. MIT Press
- Müller W., Grappin R., 2005, *Phys. Rev. Lett.*, 95, 114502
- Müller W.-C., Biskamp D., Grappin R., 2003, *Phys. Rev. E*, 67, 066302
- Osman K. T., Horbury T. S., 2007, *ApJ*, 654, L103
- Osman K. T., Horbury T. S., 2009, *Ann. Geophys.*, 27, 3019
- Oughton S., Priest E. R., Matthaeus W. H., 1994, *J. Fluid Mech.*, 280, 95
- Perez J. C., Boldyrev S., 2008, *ApJ*, 672, L61
- Perez J. C., Boldyrev S., 2009, *Phys. Rev. Lett.*, 102, 025003
- Podesta J. J., 2009, *ApJ*, 698, 986
- Podesta J. J., Bhattacharjee A., 2010, *ApJ*, 718, 1151
- Podesta J. J., Chandran B. D. G., Bhattacharjee A., Roberts D. A., Goldstein M. L., 2009, *J. Geophys. Res.*, 114, 1107
- Podesta J. J., Roberts D. A., Goldstein M. L., 2007, *ApJ*, 664, 543
- Rème H., Aoustin C., Bosqued J. M., Dandouras I., et al. 2001, *Ann. Geophys.*, 19, 1303
- Salem C., Mangeney A., Bale S. D., Veltri P., 2009, *ApJ*, 702, 537
- Sari J. W., Valley G. C., 1976, *J. Geophys. Res.*, 81, 5489
- Schekochihin A. A., Cowley S. C., Dorland W., Hammett G. W., Howes G. G., Quataert E., Tatsuno T., 2009, *ApJS*, 182, 310
- Shebalin J. V., Matthaeus W. H., Montgomery D., 1983, *J. Plasma Phys.*, 29, 525
- Smith C. W., Vasquez B. J., Hamilton K., 2006, *J. Geophys. Res.*, 111, 9111
- Strauss H. R., 1976, *Phys. Fluids*, 19, 134
- Tessein J. A., Smith C. W., MacBride B. T., Matthaeus W. H., Forman M. A., Borovsky J. E., 2009, *ApJ*, 692, 684
- Weygand J. M., Matthaeus W. H., Dasso S., Kivelson M. G., Kistler L. M., Moukic C., 2009, *J. Geophys. Res.*, 114, 7213
- Wicks R. T., Horbury T. S., Chen C. H. K., Schekochihin A. A., 2010, *MNRAS*, 407, L31